Engineering 28 (2023) 166–178

Contents lists available at ScienceDirect

Engineering

journal homepage: www.elsevier.com/locate/eng

Research
Bioengineering—Article

Remodeling Isoprene Pyrophosphate Metabolism for Promoting Terpenoids Bioproduction

Xianhao Xu [a,b], Xueqin Lv [a,b], Shixiu Cui [a,b], Yanfeng Liu [a,b], Hongzhi Xia [c], Jianghua Li [a,b], Guocheng Du [a,b], Zhaofeng Li [d], Rodrigo Ledesma-Amaro [e], Jian Chen [b,*], Long Liu [a,b,*]

[a] Key Laboratory of Carbohydrate Chemistry and Biotechnology, Ministry of Education, Jiangnan University, Wuxi 214122, China
[b] Science Center for Future Foods, Ministry of Education, Jiangnan University, Wuxi 214122, China
[c] Richen Bioengineering Co., Ltd., Nantong 226000, China
[d] State Key Laboratory of Food Science and Technology, Jiangnan University, Wuxi 214122, China
[e] Department of Bioengineering and Centre for Synthetic Biology, Imperial College London, London SW7 2AZ, UK

ARTICLE INFO

Article history:
Received 10 June 2022
Revised 28 December 2022
Accepted 21 March 2023
Available online 25 July 2023

Keywords:
Terpenoids
Genetic circuits
Bacillus subtilis
Isoprene pyrophosphate

ABSTRACT

Terpenoids are the largest family of natural products. They are made from the building block isoprene pyrophosphate (IPP), and their bioproduction using engineered cell factories has received a great deal of attention. To date, the insufficient metabolic supply of IPP remains a great challenge for the efficient synthesis of terpenoids. In this work, we discover that the imbalanced metabolic flux distribution between the central metabolism and the IPP supply hinders IPP accumulation in *Bacillus subtilis* (*B. subtilis*). Therefore, we remodel the IPP metabolism using a series of genetically encoded two-input-multi-output (TIMO) circuits that are responsive to pyruvate or/and malonyl-CoA, resulting in an IPP pool that is significantly increased by up to four-fold. As a proof-of-concept validation, we design an IPP metabolism remodeling strategy to improve the production of three valuable terpenoids, including menaquinone-7 (MK-7, 4.1-fold), lycopene (9-fold), and β-carotene (0.9-fold). In particular, the titer of MK-7 in a 50-L bioreactor reached 1549.6 mg·L^{-1}, representing the highest titer reported so far. Thus, we propose a TIMO genetic circuits-assisted IPP metabolism remodeling framework that can be generally used for the synergistic fine-tuning of complicated metabolic modules to achieve the efficient bioproduction of terpenoids.

1. Introduction

Terpenoids, which are the largest family of natural products, have a wide range of applications in the fields of pharmaceuticals, flavors, and food additives [1,2]. However, most natural producer organisms—mainly plants—are not suitable for the large-scale synthesis of terpenoids, due to their low abundance, lack of genetic manipulation tools, and long growth cycles. Conversely, the use of engineered microbial cell factories is a promising and sustainable route for the production of terpenoids [3,4]. The metabolic network related to terpenoids can be divided into three modules: the central metabolism module, isoprene pyrophosphate (IPP) supply module, and terpenoids synthesis module. IPP is the basic building block for terpenoid biosynthesis. There are two distinct natural IPP biosynthetic modules: the 2-C-methyl-D-erythritol 4-phosphate (MEP) module (present in bacteria and plants), using pyruvate and glyceraldehyde-3-phosphate as precursors, and the mevalonate (MVA) module (present in eukaryote and archaea), using acetyl-CoA as the precursor [3]. In most microbial cell factories, insufficient IPP supply limits the overproduction of terpenoids; therefore, strategies to improve their production are required. However, tuning the metabolite flux distribution between the central metabolism and IPP synthesis remains a challenge for metabolic engineering [5].

Various strategies have been proposed to enhance IPP supply, such as central metabolism engineering [6] and rate-limiting enzyme engineering [7,8]. For example, Lv et al. [9] significantly improved the synthesis of isoprene by enhancing the supply of acetyl-CoA and upregulating the expression of rate-limiting enzymes in the MVA pathway. In addition, the heterologous

* Corresponding authors.
E-mail addresses: jchen@jiangnan.edu.cn (J. Chen), longliu@jiangnan.edu.cn (L. Liu).

https://doi.org/10.1016/j.eng.2023.03.019

introduction of the MVA pathway in *Escherichia coli* (*E. coli*) was shown to trigger synergism between the MVA and MEP pathways, thereby increasing the supply of IPP [10]. However, these static regulatory strategies may lead to the accumulation of toxic intermediates, metabolic imbalance, and the generation of a new metabolic bottleneck—issues that compromise the titer, yield, and productivity of terpenoids.

Recently, synthetic genetic circuits have been proposed to mimic natural regulatory mechanisms and perform dynamic control of metabolic fluxes in response to either intracellular or extracellular signals such as temperature, light, oxygen, and intermediate metabolites [11–13]. Dynamic regulation is able to balance and fine-tune intracellular metabolic fluxes in real time according to the metabolic state of the cell, which prevents the accumulation of intermediate metabolites and promotes the efficient synthesis of products [12]. Based on the IPP-responsive genetic circuit, Chou and Keasling [14] designed an adaptive evolutionary system that significantly increased the production of terpenoids. Moreover, Zhou et al. [15] developed a naringenin-coumaric acid-malonyl-CoA-balanced (NCOMB) genetic circuit for dynamic control of the precursor malonyl-CoA. Although these genetic circuits can improve the synthesis of terpenoids to a certain degree, they are independent of each other, are single-input, focus on one target, and do not synergistically regulate the IPP metabolism, resulting in restricted IPP supply and product titers.

In this work, a genetically encoded two-input-multi-output (TIMO) circuits-assisted framework is proposed for remodeling the IPP metabolism (Fig. 1). As a proof of concept, we engineer *Bacillus subtilis* (*B. subtilis*) to produce menaquinone-7 (MK-7), which is a valuable terpenoid used to prevent osteoporosis, arterial calcification, and Parkinson's disease [16]. First, we introduce an MVA module into an MK-7-producing strain, BS17 [17], to enhance IPP accumulation, thereby obtaining the strain BS17-MVA. Subsequently, we identify the bottleneck limiting the IPP supply by measuring the content of intracellular metabolites in the strain BS17-MVA (Fig. 1(a)), and then design a cascade regulatory system for the synergistic regulation of IPP metabolism (Fig. 1(b)). Next, according to the designed cascade regulatory system, we build a series of bifunctional malonyl-CoA-responsive genetic circuits and a two-input AND gate and OR gate in response to malonyl-CoA and pyruvate based on the transcriptional factor FapR, PdhR, and antisense transcription (Figs. 1(c) and (d)). Finally, we introduce these genetically encoded circuits into BS17-MVA to dynamically remodel the central metabolic module and IPP supply module (Fig. 1(e)). The engineered strain expressing the TIMO genetic circuits can produce up to 1549.6 mg·L^{-1} MK-7 in a 50-L bioreactor, which is the highest MK-7 titer reported so far. Moreover, we validate the application of the proposed framework in the production of two other valuable terpenoids: lycopene and β-carotene (Fig. 1(f)).

2. Material and methods

2.1. Strains, plasmids, and cultivation conditions

The strains, plasmids, and primers involved in this study are listed in Tables S1–S3 in Appendix A. *E. coli* was cultivated in Luria-Bertani (LB) medium at 37 °C and 100 μg·mL^{-1} ampicillin was supplemented when required. The fermentation medium of *B. subtilis* for MK-7 production was composed of 50 g·L^{-1} glucose,

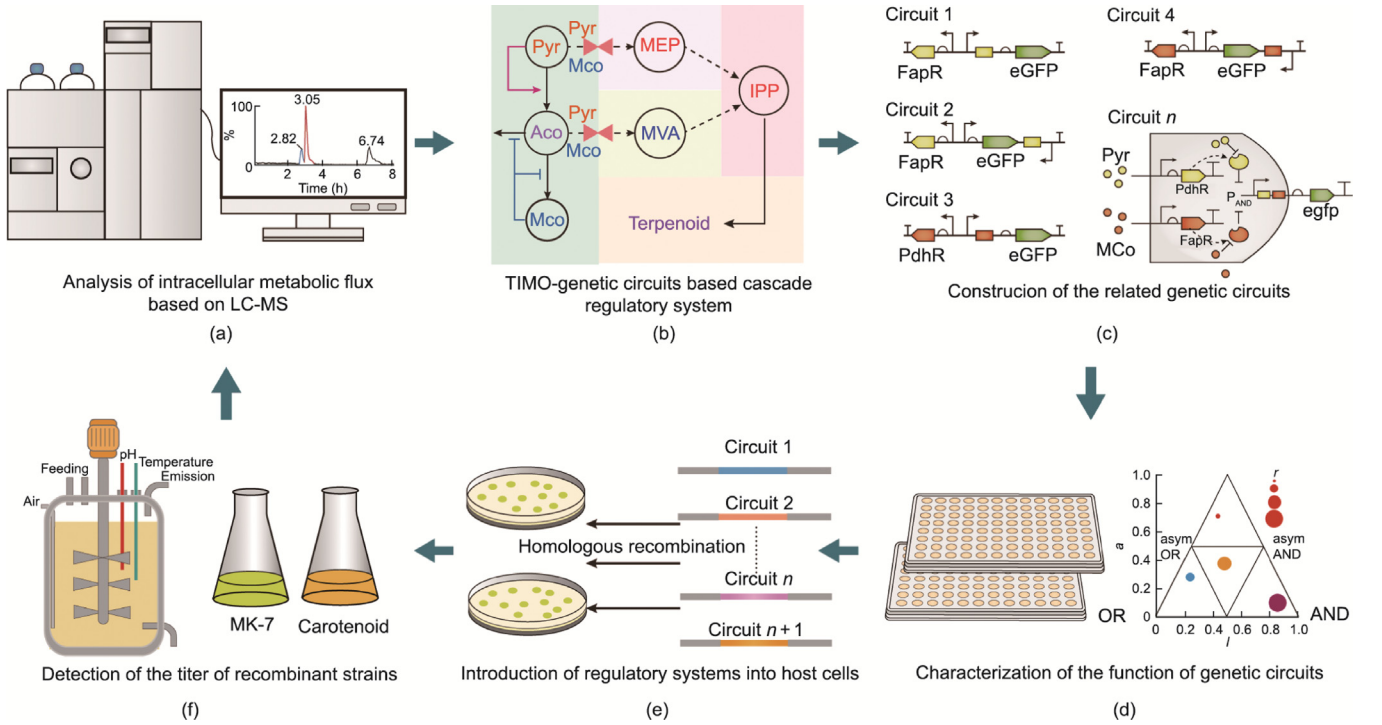

Fig. 1. Framework for the TIMO genetic circuit-assisted strategy for remodeling and synergistic regulating IPP metabolism. (a) Liquid chromatography-mass spectrometry (LC-MS) was used to detect the content of key intracellular metabolites, including MVA, MEP, pyruvate, and acetyl-CoA. Thus, the intracellular metabolic flux distribution was analyzed. (b) According to the analysis results, the corresponding regulatory system based on the genetic circuit cascade was designed to facilitate the flow of metabolic fluxes into the IPP supply module. Pyr: pyruvate; Aco: acetyl-CoA; Mco: malonyl-CoA. Pink arrow, pyruvate activated genetic circuit; blue blunt-end arrow: malonyl-CoA-inhibited genetic circuit; switch, AND/OR gate in response to pyruvate and malonyl-CoA. (c) The genetic circuits involved in the regulatory system were constructed separately, including one-input genetic circuits and two-input genetic circuits. eGFP: enhanced green fluorescence protein; FapR: malonyl-CoA-responsive transcriptional factor; PdhR: pyruvate-responsive transcriptional factor. (d) The performance and logic behavior of these genetic circuits were characterized and optimized, including the dynamic range, responsive threshold, and specificity. *r*: dynamic range; *a*: the asymmetry of the gate with respect to its two inducers; *l*: the logical behavior of the promoter; asym: asymmetry. (e) The optimized genetic circuits were introduced into the host to build a regulatory system for regulating IPP metabolism. (f) The product yield and intracellular metabolite content of the recombinant strain in a shake flask and bioreactor were detected.

50 g·L^{-1} soy peptone, 50 g·L^{-1} yeast extract, and 0.6 g·L^{-1} KH_2PO_4. Appropriate antibiotics were added to the culture medium as required: kanamycin (50 μg·mL^{-1}), spectinomycin (50 μg·mL^{-1}), zeocin (40 μg·mL^{-1}), and chloramphenicol (5 μg·mL^{-1}). Chemical reagents were purchased from Sigma-Aldrich (USA) or Sinopharm Chemical Reagent Co., Ltd. (China).

2.2. DNA manipulation

For the construction of the malonyl-CoA-responsive genetic circuits, the plasmid pHT01-P43-GFP was first linearized using the primer Zai_fapRF/R. Then, the promoters P_{fabHA}, P_{fabHB}, and P_{fabI} were cloned from the genome of *B. subtilis* 168 with the primer pairs fabHAF/R, fabHBF/R, and fabIF/R, respectively, and the fragments were fused using a Gibson Assembly Cloning Kit (NEB, UK) to obtain the plasmids pHT01-fabHA-GFP, PHT01-fabHB-GFP, and pHT01-fabI-GFP. To construct the plasmids pHT01-P43FU-GFP, pHT01-P43FD-GFP, and pHT01-P43F1-GFP, the FapR binding site (5′-AATTATATACTACTATTAGTACCTAGTCTTAATT-3′) was inserted into plasmid pHT01-P43-GFP using reverse polymerase chain reaction (PCR) and the primer pairs FapRU-F/R, FapRD-F/R, and FapR1-F/R, respectively. For the construction of the plasmid pHT01-Pveg-fapR-fabI-GFP, the plasmid pHT01-P43-GFP was linearized using the primer Zai_VegF/R, and P_{veg}, P_{fabI}, and *fapR* were cloned from the genome of *B. subtilis* 168 with the primer pairs PvegF/R, FabI_-VegF/R, and FapR_vegF/R, respectively. Finally, the fragments were fused using Gibson Assembly. A FapR binding site mutation library was constructed by the degenerate primer pairs P43FDTUF/R, and pHT01-P43FD-GFP was used as a template. Then, the PCR product was digested by *Dpn*I (NEB) and transformed into *E. coli* JM109 Competent Cells (Takara, Japan). The construction procedures of the plasmids pHT01-PxylA-fapR-fabI-GFP and pHT01-PxylA-fapR-P43FD180-GFP were similar to those of pHT01-Pveg-fapR-fabI-GFP. Promoter P_{xylA} was cloned from the plasmid pStop using the primer pair PIAN_xylAF/R.

For the construction of the antisense malonyl-CoA-responsive circuits, the following procedure was followed. To construct the plasmid pHT01-GAP-GFP, PGAP was cloned from the genome of *E. coli* K12 using the primer pair P_GAPF/R and was then inserted into pHT01-P43-GFP using Gibson Assembly. To construct the antisense malonyl-CoA sensor, first, the plasmid pHT01-grac100 was linearized using the primer Fan_ZaiF/R. Then, the promoter P_{fabI}, P43FD, and P43FD180 were cloned from the corresponding plasmid using the primer pairs Fan_fabIF/R and Fan_180DF/R, respectively. Finally, these fragments were fused using Gibson Assembly. Reverse PCR was used to remove the promoter core region in the plasmids pHT01-grac100-fabI, pHT01-grac100-P43FD, and pHT01-grac100-P43FD180, and Qu_fabIF/R, Qu_DF/R, and Qu_180DF/R were respectively used as the primer pairs. The construction procedure of the antisense promoter library was similar to that of the FapR binding site mutation library, and Tu_-fabIGF/R were used as degenerate primer pairs.

The construction of the two-input logic gate was done in the following way: To construct the plasmids AyteJM-P43FD180 and AyteJU-P43FD180, a FapR binding site was inserted into the plasmids pHT01-yteJM-GFP and pHT01-yteJU-GFP using the primer pairs Yu_yteJMF/R and Yu_yteJUF/R, respectively. To construct the plasmids AyteJMG-P43FD180 and AyteJUG-P43FD180, the plasmids AyteJM-P43FD180 and AyteJU-P43FD180 were used as templates, and Pgrac100MF/R and Pgrac100UF/R were used as primer pairs. To optimize the distance between the PdhR binding site and the –35 region of the plasmids AyteJU-P43FD180 and AyteJUG-P43FD180, the primer pairs YteJ_(1/2/3/4/5/6/7/8/9/10) UF/R and grac100_(1/2/3/4/5/6/7/8/9/10) UF/R were used. To construct the plasmids OyteJU-P43FD180 and OP43FD180-yteJU, the promoter P43FD180 was inserted into the up or downstream of the promoter yteJU in the plasmid pHT01-yteJU-GFP using the primer pairs UP_P180F/R and DP_P180F/R, respectively. To optimize the distance between the promoters P43FD180 and yteJU, different lengths of *yeeZ* (GenBank ID: 946538) gene fragments were cloned from the *E. coli* K12 genome using the primer pairs 100_F/(100/200/300/400/500) R and were inserted into OyteJU-P43FD180 using Gibson Assembly.

2.3. Strain construction

All molecular biology manipulations of *B. subtilis* were performed as previously described [18]. 168-ΔFapR was constructed by deleting the *fapR* gene in *B. subtilis* 168. The gene *pdhR* (GenBank ID: 944827) used to construct the strains PR and PR-ΔfapR was cloned from the genome *E. coli* K12. In order to replace the P43 promoter of the gene *pdhR* in the strain PR, the promoters P_{gsiB}, P_{veg}, and P43D1 were cloned from *B. subtilis* and the plasmid pHT01-P43-GFP, respectively, and the strains Pveg-PR, PgsiB-PR, and P43D1-PR were obtained.

The construction of the MVA pathway in BS17 was done according to the following procedure. First, the genes *mvaE* (encoding acetoacetyl-CoA thiolase; GenBank ID: AF290092) and *mvaS* (encoding MVA synthase; GenBank ID: AF290092) from *Enterococcus faecalis*, and the gene *mk* (encoding MVA Kinase; GenBank ID: AAM31458) from *Methanosarcina mazei* were synthesized and codon optimized in Genewiz (China). Then, the genes *pmK* (encoding phosphomevalonate kinase; GenBank ID: 855260) and *pmD* (encoding diphosphate MVA decarboxylase; GenBank ID: 855779) were cloned from the genome of *Saccharomyces cerevisiae* (*S. cerevisiae*). Finally, these genes were integrated into the genome of BS17 and expressed using the promoter P43 to obtain the recombinant strain BS17-MVA.

For dynamic control of the MK-7 metabolic network in BS17-MVA, the gene *pdhR* was integrated into the genome of BS17-MVA, yielding the strain BS17-P. As a control, the *fapR* gene in the statically regulated strain was knocked out to obtain the strain BS17-F. Then, pyruvate-activated promoters (D11 and D6) were used to replace the native promoter of the gene *pdhA* in the strain BS17-P, yielding the strains BS17-P1 and P2. Similarly, a pyruvate-activated promoter (D11) was used to replace the native promoter of the gene *pdhA* in the strain BS17-F, yielding the strain BS17-F1. Subsequently, malonyl-CoA-inhibited promoters (FabIG18-5 and FabIG12-29) were inserted into the 3′ end of the genes *accA* and *citZ* to obtain the corresponding dynamically and statically regulated strain. Similarly, the pyruvate-malonyl-CoA 2-input AND gates (AyteJM-P43FD180, AyteJU9-P43FD180, and AyteJUG2-P43FD180) or OR gates (OyteJU-P43FD180, OyteJU300-P43FD180, and OyteJU500-P43FD180) were used to replace the original promoter P43 of the genes *mvaE*, *dxs*, and *hepS*, yielding the corresponding dynamically and statically regulated strains (Table S3 in Appendix A).

The construction of the β-carotene biosynthesis pathway in BS17-MVA and BS17-P13 was done as follows. First, the genes *crtE* (encoding geranylgeranyl diphosphate synthase; GenBank ID: 69517638), *crtB* (encoding phytoene synthase; EMBL ID: GU721093.1), *crtI* (encoding phytoene desaturase; GenBank ID: 66827556), and *crtY* (encoding lycopene β-cyclase; EMBL ID: GU721093) in *Erwinia herbicola* (*E. herbicola*) Eho10 were cloned from the plasmid pAC-BETAipi (purchased from Addgene). Then, the promoter P_{veg} was cloned from the genome of *B. subtilis*. Next, the genes *crtE, crtB, crtI*, *crtY*, and P_{veg} were inserted into the plasmid pHT01-P43-GFP using a Gibson Assembly Cloning Kit, yielding the plasmid pHT01-Beta. Finally, the plasmid pHT01-Beta was transformed into the strains BS17-MVA and BS17-P13, resulting in the strains MVA-Beta and P13-Beta.

2.4. Construction of the FapR mutation library and the site-directed saturation mutation of FapR

The FapR mutation library was constructed using a QuickMutation Random Mutagenesis Kit (Beyotime, China). Three consecutive rounds of error-prone PCR (epPCR) were carried out using the primer pairs FapRF/R. The PCR product of each round of epPCR was purified and used to replace the wild-type *fapR* gene in the plasmid pHT01-PxylA-fapR-P43FD180-GFP using Gibson Assembly. Then, the assembly product was digested by *Dpn*I (NEB) and transformed into *E. coli* JM109 Competent Cells (Takara). Next, the plasmid library was extracted from *E. coli* and further transformed into 168-ΔFapR, producing the FapR mutation library. Using the plasmid pHT01-PxylA-fapR-P43F180D-GFP as a template, reverse PCR was used to carry out site-directed saturation mutation of Arg106 in FapR; the primers used were FapR106F and FapR106R.

2.5. Fluorescence measurements and flow cytometry

To detect the fluorescence intensity of strains with different genetic circuits, the strain was first streaked into an LB solid plate containing 5 μg·mL^{-1} chloramphenicol and cultured at 37 °C for 12 h. Then, a single colony was picked into 2 mL of LB medium containing 5 μg·mL^{-1} chloramphenicol and cultured at 37 °C for 12 h. Next, 4 μL of culture was incubated in a 96-well fluorescent plate containing 200 μL of LB medium with 5 μg·mL^{-1} chloramphenicol. In addition, 5 g·L^{-1} inducer, 50 μmol·L^{-1} IPTG, and 10 μg·mL^{-1} cerulenin were added to the culture medium as required. The eGFP (enhanced green fluorescent protein) fluorescence (excitation, 488 nm; emission, 520 nm) and OD_{600} were detected by means of a Cytation microplate reader (BioTek, USA).

For all sorting steps, *B. subtilis* with a different mutation library were thawed from −80 °C, incubated (1%, v/v) into 10 mL of liquid LB medium with 5 μg·mL^{-1} chloramphenicol, and cultured at 37 °C for 12 h. Then, 2% (v/v) cells were incubated in 50 mL of liquid LB medium containing 5 μg·mL^{-1} chloramphenicol (10 μg·mL^{-1} cerulenin was added to the culture medium as required), and cultured at 37 °C and 220 r·min^{-1} for 16 h. Next, 1 mL of the cultured cells was rinsed twice with 1×phosphate-buffered saline (PBS; NaCl 0.8%, KCl 0.02%, Na_2HPO_4 0.144%, and KH_2PO_4 0.024%, pH 7.4), and then resuspended in 1×PBS to an OD_{600} of 0.6. Finally, 20 000 variants were sorted using flow cytometry (BD FACSArica III, USA) according to their fluorescence intensity. The data on fluorescence intensity was analyzed using the software FlowJo VX10.

2.6. Mathematical model of logic behavior

The logic behavior of the logic gates was characterized using the model developed by Cox et al. [19]. Three parameters are defined in the model: *r*: the dynamic range of the logic gate; *a*: the asymmetry of the logic gate that quantifies the inhibitory effect of each transcription factor on the logic gate, where a greater *a* value means that the gate is only regulated by one of the two transcription factors; and *l*: the logic behavior of the gate. The values of *a* and *l* vary between 0 and 1. A pure AND gate is characterized by $a = 0$ and $l = 1$, while a pure OR gate is characterized by $a = l = 0$. The parameters *a*, *l*, and *r* were calculated by means of the following equations:

$$r = \frac{\mathrm{GFP(IV)}}{\mathrm{GFP(I)}} \tag{1}$$

$$l = \frac{2 \times \log_{10}(\mathrm{IV}) - \log_{10}(\mathrm{II} \times \mathrm{III})}{2 \times \log_{10}(r)} \tag{2}$$

$$a = \frac{\log_{10}(\mathrm{III}) - \log_{10}(\mathrm{II})}{\log_{10}(r)} \tag{3}$$

The relative fluorescence intensity of the gate under different conditions (i.e., no transcriptional factors, FapR only, PdhR only, FapR+PdhR) was ordered from highest to lowest and labeled as follows: IV ≥ III ≥ II ≥ I.

2.7. Reverse-transcriptase PCR analysis

For the quantitative reverse-transcriptase PCR (qRT-PCR) analysis, 1 mL of cells from the culture medium was first frozen in liquid nitrogen. Then, the total RNA of the cells was extracted using an RNeasy Mini Kit (Qiagen, China). Next, complementary DNA (cDNA) was synthesized using a PrimeScript RT-PCR kit (Takara). The qRT-PCR was performed using TB Green Premix Ex Taq II (Takara) and carried out in a LightCycler 480 II real-time PCR instrument (Roche Applied Science, Germany). The gene *16sRNA* was selected as the internal standard.

2.8. MK-7 and β-carotene production in a shake flask and 50-L bioreactor

The production of MK-7 and β-carotene in a shake flask was carried out as follows. First, the strain was streaked into an LB solid plate and cultured at 37 °C for 12 h. Then, a single clone was picked into 10 mL of LB medium in a 50-mL tube at 37 °C and 220 r·min^{-1}. Next, 1 mL of overnight-cultured cells (12 h) were inoculated with 15 mL of fermentation medium (50 g·L^{-1} glucose, 50 g·L^{-1} soy peptone, 50 g·L^{-1} yeast extract, and 0.6 g·L^{-1} KH_2PO_4) in 250 mL shake flasks at 40 °C and 220 r·min^{-1} for 5 days.

The production of MK-7 in a 50-L bioreactor was carried out as follows. First, the strain was streaked into an LB solid plate and cultured at 37 °C for 12 h. Then, single clone was picked into 500 mL LB medium and cultured in 2-L shake flasks at 37 °C and 220 r·min^{-1} for 12 h. Next, 8% (v/v) overnight culture cells were inoculated with 30 L of fermentation medium (50 g·L^{-1} glucose, 5 g·L^{-1} soy peptone, 50 g·L^{-1} yeast extract, and 0.6 g·L^{-1} KH_2PO_4) in a 50-L bioreactor. The concentration of dissolved oxygen (DO) was controlled in the range of 40%–60%, and the fermentation temperature was 40 °C. The glucose concentration was maintained in the range of 20–30 g·L^{-1}.

2.9. MK-7 and intracellular metabolite content detection method

From the fermentation culture, 0.5 mL of cells was added to 2 mL of MK-7 extract buffer (2-propanol:*n*-hexane = 1:2) to extract the MK-7. Then, the mixture was shaken on a vortex shaker for 10 min and centrifuged at 6000*g* for 5 min. The supernatant of the mixture was used to detect the titer of MK-7. High-performance liquid chromatography (HPLC) was used to detect the titer of MK-7. The instrument was an Agilent 1260 series, the column was a C18 ODS column (5 μm, 250 mm × 4.6 mm; Thermo Fisher Scientific, USA), and the column temperature was 40 °C. The mobile phase was methanol:dichloromethane (9:1, v/v), and the flow rate was 1 mL·min^{-1}. The HPLC data was collected and analyzed using the Agilent OpenLAB Control Panel.

The concentration of glucose in the fermentation culture was detected using a glucose-lactate analyzer (M100; Shenzhen Sieman Technology Co., Ltd., China). The concentration of intracellular pyruvate was detected using a Micro Pyruvate Acid (PA) Assay Kit (Solarbio, China). To measure the concentration of intracellular acetyl-CoA, malonyl-CoA, MEP, and MVA, 3 mL of cells from the culture medium was frozen in liquid nitrogen. The cells were then thawed, rinsed twice with an equal volume of sterile water, and then resuspend in 3 mL of sterile water. Next, 12 mL of precooled extraction solution (acetonitrile:methanol:water = 4:4:2) was added, and intracellular metabolites were extracted at 4 °C for 16 h. Subsequently, the cell supernatant was collected by centrifu-

gation at 9000*g* for 10 min, and then lyophilized in a freeze dryer (Labconco, USA). The lyophilized powder was redissolved in 100 μL of ultrapure water, and the supernatant was collected by centrifugation at 9000*g* for 10 min. High-performance liquid chromatography-mass spectrometry (LC-MS) was used to detect the concentrations of intracellular metabolites.

LC-MS/MS was used to detect the content of MEP and IPP. A Luna 3 μm NH_2 column (150 mm × 2 mm, 3 μm) was used as the column. Mobile phase A was H_2O:acetonitrile (95:5, containing 20 mm of NH_4HCO_3, pH = 9.5), and the mobile phase B was acetonitrile. The flow rate was 0.2 mL·min^{-1}. The HPLC condition was as follows: 0–1 min, 20% A; 1–30 min, 20%A–100%A; 30–31 min, 100%A; 31–31.1 min, 100%A–20%A; 31.1–40 min, 20%A. The column temperature was 30 °C. The MS condition was negative mode and full scan. The LC-MS data were collected and analyzed using MassLynx V4.1. The detection instrument was a Waters Maldi Synapt Q-ToF MS (USA). Detection of the acetyl-CoA and malonyl-CoA content followed the procedure described by Onorato et al. [20], detection of the MVA content followed the procedure described by Kindt et al. [21], and detection of the MEP content followed the procedure described by Buescher et al. [22]. The LC-MS data were collected and analyzed by means of MassLynx V4.1.

2.10. Statistical analysis

Three independent replicates were performed for all experiments. A statistical data analysis was performed with *t*-texts in SPSS 25.0. *P* values of < 0.05 were considered to be statistically significant, and statistical significance is indicated as * for $p < 0.05$ and as ** for $p < 0.01$.

3. Results

3.1. Enhancing the IPP supply via heterologous introduction of an MVA module

In our previous study, we constructed an MK-7-producing strain, BS17, by overexpressing the rate-limiting enzymes in *B. subtilis* to enhance the IPP supply (0.27 nmol·g^{-1} dry cell weight (DCW)), including 1-deoxy-D-xylulose-5-phosphate synthase (Dxs) and 1-deoxyxylulose-5-phosphate reductoisomerase (Dxr) [17]. Gao et al. [23] found that introducing a heterologous MVA module into *E. coli* significantly increased the IPP supply and MK-7 production. To further enhance the supply of IPP, we herein introduced an MVA module into the strain BS17. In particular, the genes *mvaE* (encoding acetoacetyl-CoA thiolase) and *mvaS* (encoding mevalonate synthase) from *Enterococcus faecalis*, the gene *mk* (encoding MVA kinase) from *Methanosarcina mazei*, and the genes *pmK* (encoding phosphomevalonate kinase) and *pmD* (encoding diphosphate mevalonate decarboxylase) from *S. cerevisiae* were integrated into the BS17 genome, yielding the strain BS17-MVA (Fig. 2(a)). The RT-PCR results show that the genes *mvaE*, *mvaS*, *mk*, *pmK*, and *pmD* were successfully transcribed in the strain BS17-MVA (Fig. 2(b)). Subsequently, we knocked out the essential gene *ispD* (encoding 2-C-methyl-D-erythritol 4-phosphocytidine transferase) of the MEP module in BS17-MVA to generate the strain BS17-MVA-ΔispD (Fig. 2(a)). The growth of strain BS17-MVA-ΔispD indicates that the MVA module was successfully expressed and is active in BS17-MVA, because the MEP is the only module responsible for IPP synthesis in *B. subtilis* (Fig. 1(a)). In addition, we found that the cell growth rate, glucose consumption rate, and MK-7 production of BS17-MVA-ΔispD were significantly lower than those of BS17 and BS17-MVA (Fig. 2(c); Figs. S1(a) and (b) in Appendix A), suggesting that only the MVA module cannot provide enough IPP for cell growth and MK-7 synthesis.

Compared with the strain BS17, the maximum OD_{600} of BS17-MVA decreased by 16%, the specific titer of MK-7 increased by 19%, the intracellular MEP (17.10 nmol·g^{-1} DCW) and IPP (0.30 nmol·g^{-1} DCW) content increased by 85% and 11%, respectively, and the concentrations of the byproducts lactic acid (0.28 g·L^{-1}) and acetic acid (1.82 g·L^{-1}) decreased by 27% and 17%, respectively (Figs. 2(d) and (e); Figs. S1(b) and (c) in Appendix A). These results demonstrate that there is a synergistic effect between the MVA module and MEP module, which can enhance the supply of IPP. We also found that the contents of intracellular pyruvate (1783.65 nmol·g^{-1} DCW) and acetyl-CoA (485.84 nmol·g^{-1} DCW) in BS17-MVA were significantly higher than those of MEP (17.10 nmol·g^{-1} DCW) and MVA (2.73 nmol·g^{-1} DCW) (Fig. 2(e)). In addition, the intracellular MEP content was significantly higher than that of MVA. These results demonstrate that the metabolic flux distribution among the central metabolism module, MEP module, and MVA module was imbalanced, limiting the overproduction of terpenoid MK-7.

Pyruvate and acetyl-CoA are the precursors of the MEP and MVA pathways. In addition, pyruvate and malonyl-CoA are two key metabolites in the cell; pyruvate is a key node connecting glycolysis and the tricarboxylic acid (TCA) cycle, while malonyl-CoA—derived from acetyl-CoA—is the precursor for lipid synthesis [24]. Therefore, we designed a TIMO genetic circuits-assisted cascade regulatory system that responds to intracellular pyruvate and malonyl-CoA for remodeling IPP metabolism (Fig. 2(f)). First, pyruvate-activated genetic circuits were used to enhance the expression of the gene *pdhA*, thereby promoting the conversion of pyruvate to acetyl-CoA when the intracellular pyruvate content is high. Then, malonyl-CoA-inhibited genetic circuits were used to inhibit the expression of the genes *accA* and *citZ*. Thus, a high intracellular pyruvate concentration inhibits the acetyl-CoA flow into the lipid synthesis pathway and TCA cycle. Later, a pyruvate-malonyl-CoA 2-input AND gate or OR gates were used to enhance the expression of the genes *dxs* and *mvaE*. Therefore, when the intracellular pyruvate and malonyl-CoA contents are high, the central metabolic flux will flow into the IPP supply module rather than promoting cell growth. Compared with the OR gate, the AND gate also balances the metabolic fluxes between the MEP module and MVA module, thereby promoting the synergism between the MEP and MVA modules. In a previous study, we constructed a series of pyruvate-responsive genetic circuits [25]. Here, we designed and built a series of bifunctional malonyl-CoA-responsive genetic circuits, a pyruvate-malonyl-CoA 2-input AND gate, and OR gates.

3.2. Design and building of malonyl-CoA-responsive genetic circuits

As a malonyl-CoA-responsive transcription factor in *B. subtilis*, FapR mainly regulates the genes involved in the fatty acid synthesis pathway, such as *fabHA* (encoding 3-oxoacyl-ACP synthase III), *fabHB* (also encoding 3-oxoacyl-ACP synthase III), and *fabI* (encoding enoyl-ACP reductase) [26]. Therefore, we first used the native promoters of *fabHA*, *fabHB*, and *fabI* to construct the malonyl-CoA-responsive genetic circuits. In parallel, we also constructed three synthetic promoters by inserting the FapR binding site into the core region of the constitutive strong promoter P43 (Fig. 3(a); Fig. S2(a) in Appendix A). The results show that the strengths of the promoters P_{fabHB}, P_{fabI}, P43FD, and P43F1 were significantly lower than those in 168-ΔfapR (with FapR knocked out), which demonstrates that the activities of the promoters P_{fabHB}, P_{fabI}, P43FD, and P43F1 were inhibited by FapR. In addition, the inhibitory effect of FapR can be relieved by adding cerulenin (a fatty acid synthesis pathway inhibitor that promotes the accumulation of malonyl-CoA) in a dose-dependent manner (Figs. 3(b) and (c);

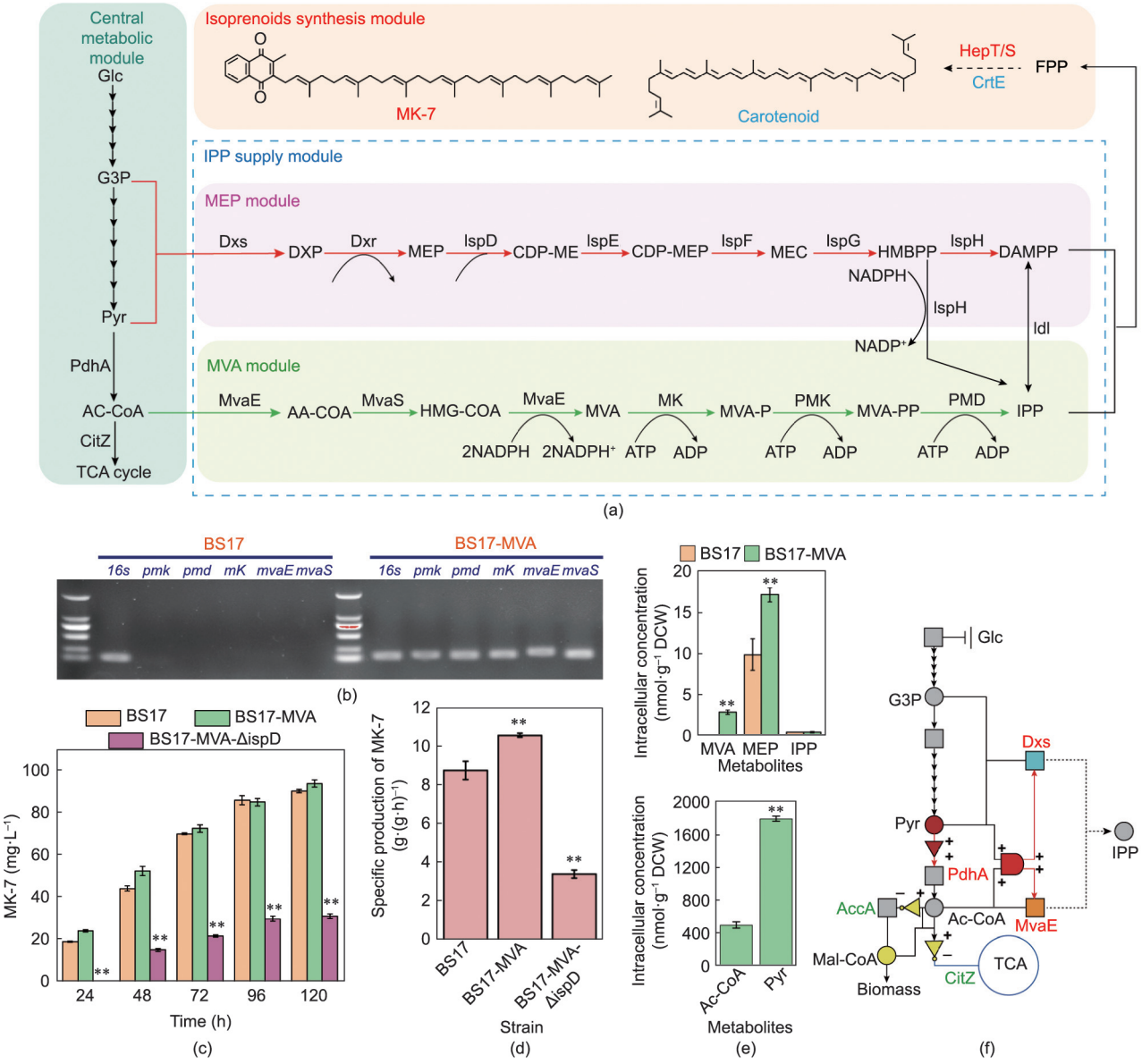

Fig. 2. Introducing the MVA pathway into *B. subtilis*. (a) Pathway of terpenoids biosynthesis in *B. subtilis*. PdhA: pyruvate dehydrogenase; CitZ: citrate synthase; IspE: 4-diphosphocytidyl-2-C-methylerythritol kinase; IspF: 2-cmethylerythritol-2,4-cyclodiphosphate synthase; IspG: 4-hydroxy-3-methylbut-2-enyldipho-sphate synthase; IspH: 4-hydroxy-3-methylbut-2-enyldiphosphate reductase; Idl: isopentenyl pyrophosphate isomerase; MvaE: acetoacetyl-CoA thiolase; HepT/S: heptamyl diphosphate synthase I/II; ispD: 2-C-methyl-D-erythritol 4-phosphocytidine transferase; MvaS: MVA synthase; MK: MVA kinase; PMK: phosphomevalonate kinase; PMD: diphosphate MVA decarboxylase; G3P: glyceraldehyde-3-phosphate; DXP: 1-deoxy-D-xylulose 5-phosphate; CDP-ME: 4-diphosphocytidyl-2C-methyl-D-erythritol; MEC: 2C-methyl-D-erythritol-2,4-cyclo-diphosphate; CDP-MEP: 4-diphosphocytidyl-2C-methyl-D-erythritol-2-phosphate; HMBPP: 4-hydroxy-3-methyl-2-(E)-butenyl-4-diphosphate; Ac-CoA: acetyl-CoA; HMG-COA: 3-hydroxy-3-methylglutaryl-CoA; AA-CoA: acetoacetyl-CoA; MVA-P: MVA-5-phosphate; MVA-PP: MVA-5-diphosphate. (b) Detecting the expression of the genes *pmk*, *pmd*, *mK*, *mvaE*, and *mvaS* in strains BS17 and BS17-MVA using RT-PCR. 16sRNA (16s) was selected as the internal standard. (c) MK-7 titer of strains BS17, BS17-MVA, and BS17-MVA-ΔispD at different fermentation times. (d) Specific production of MK-7 in different strains. (e) Intracellular content of MVA, MEP, IPP, acetyl-CoA, and pyruvate in strains BS17 and BS17-MVA. (f) Schematic diagram of the construction of the cascade regulatory system for IPP biosynthesis. The pyruvate-activated genetic circuit enhanced the conversion of pyruvate to acetyl-CoA, thereby balancing the supply of precursors for the MVA and MEP pathways. The malonyl-CoA-inhibitory genetic circuit inhibited the carbon metabolism flow into the fatty acid synthesis pathway and the TCA cycle. The two-input AND or OR gate in response to pyruvate and malonyl-CoA controlled the opening of the MVA and MEP pathways. When the content of intracellular pyruvate and malonyl-CoA is high, the carbon source flow to the central metabolism is inhibited and its flow into the IPP supply module is promoted AccA: acetyl-CoA carboxylase. Data displayed as mean ± s.d. (n = 3). The statistical analysis is based on Student's t-test. All data were the average of three independent experiments with standard deviations. * and ** indicate $p < 0.05$ and $p < 0.01$, respectively.

Figs. S2(b)–(e) in Appendix A). Moreover, when FapR was expressed on a plasmid, the activity of P_{fabI} decreased significantly, and cerulenin could no longer completely relieve the inhibitory effect of FapR (Fig. S3 in Appendix A). This finding indicates that the binding ability between FapR and its binding site is relatively weak, which may limit the dynamic range of the genetic circuit.

Then, we detected the response threshold of the malonyl-CoA-response genetic circuit by adding different contents of cerulenin. The results show that the concentration of intracellular malonyl-CoA gradually increased with the increase in the content of cerulenin (Fig. 3(d); Fig. S4(a) in Appendix A). In addition, the relative fluorescence intensity of the genetic circuit showed a dose-dependent response of malonyl-CoA, with a response threshold of 50–130 nmol·g^{-1} DCW (Fig. 3(e)). Moreover, we found that adding glucose—a commonly used carbon source—promoted the accumulation of intracellular malonyl-CoA and activated the genetic

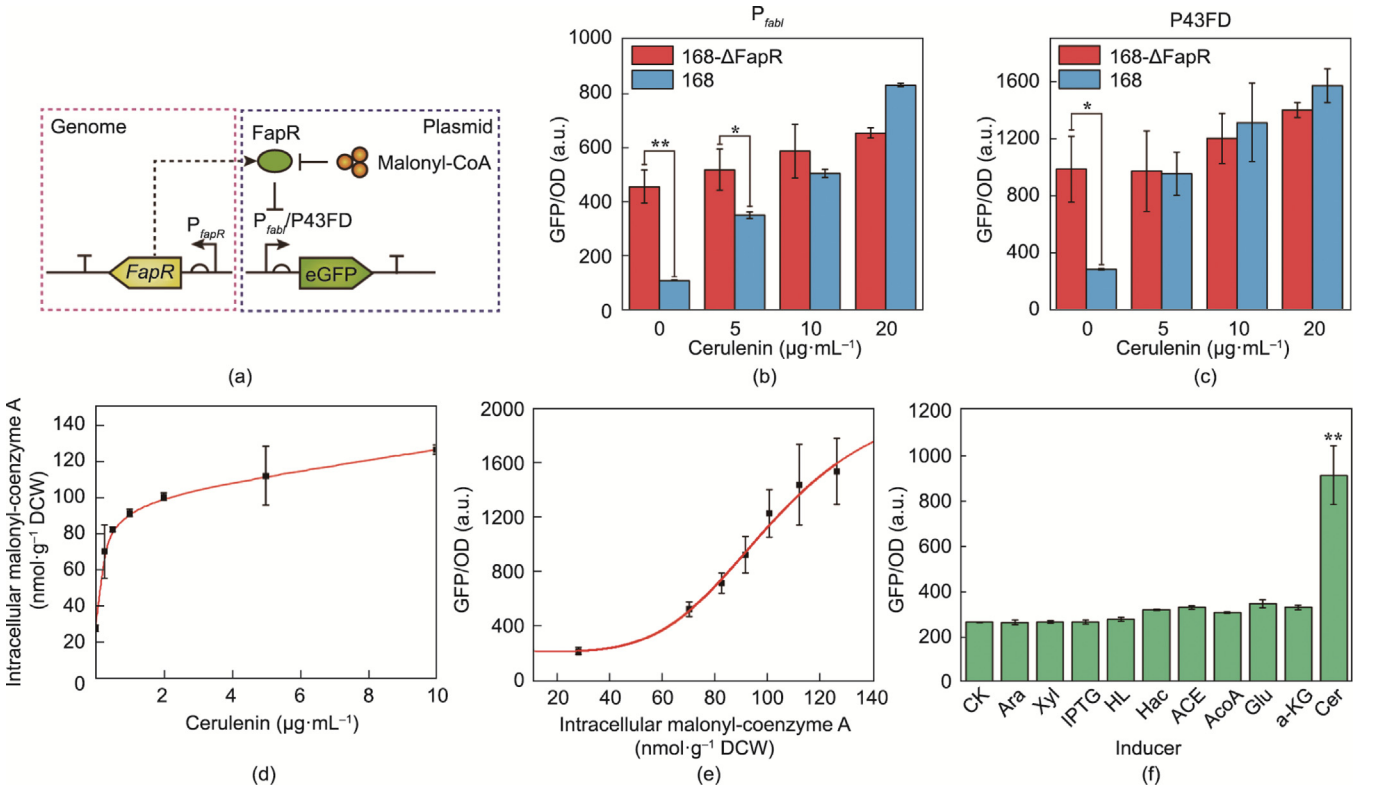

Fig. 3. Construction and characteristics of FapR-based malonyl-CoA-responsive genetic circuits. (a) Schematic diagram of the construction of malonyl-CoA-responsive genetic circuits. Malonyl-CoA-responsive transcription factor FapR was expressed using its native promoter (P_{fapR}) on the genome. P_{fabI}: a native promoter of the gene *fabI*; P43FD: the hybrid promoter that the FapR binding site was inserted into the downstream of the "−35" region of the promoter P43; eGFP: enhanced green fluorescence protein (reporter)). (b, c) Strength of the promoters (b) P_{fabI} and (c) P43FD in the strains with (168) or without (168-ΔFapR) FapR, respectively, when adding different concentrations of cerulenin, GFP/OD, relative fluorescent intensity. (d) Addition of cerulenin to the culture medium leads to increased intracellular malonyl-CoA. (e) FapR-inhibited P43FD transcriptional activity was upregulated by increasing the levels of intracellular malonyl-CoA. (f) Transcriptional activity of the FapR-inhibited promoter P43FD under different inducers. CK: no inducer; Ara: arabinose; Xyl: xylose; IPTG: β-D-1-thiogalactopyranoside; HL: lactate; HAc: acetic acid; ACE: acetoin; AcoA: acetyl-CoA; Glu: glutamate; a-KG: ketoglutaric acid; Cer: cerulenin. Data displayed as mean ± s.d. (n = 3). The statistical analysis is based on Student's t-test. All data were the average of three independent experiments with standard deviations. * and ** indicate $p < 0.05$ and $p < 0.01$, respectively.

circuits (Fig. S4(b)). Furthermore, we examined the orthogonality of the genetic circuit and found that it has a high specificity for malonyl-CoA (Fig. 3(f)).

3.3. Optimization of the dynamic range and response threshold of malonyl-CoA-responsive genetic circuits

Genetic circuits with different dynamic ranges can be used to fine-tune the expression level of target genes. Since it was found that the binding sequence of FapR affects the dynamic range of the genetic circuits, we expected to obtain genetic circuits with different dynamic ranges by constructing mutation libraries of the synthetic promoter P43FD (Fig. S5 in Appendix A). First, reverse PCR was used to introduce mutations into the FapR binding site. Subsequently, a flow cytometer was used to sort the variants with higher fluorescence intensity when 10 μg·mL^{-1} cerulenin was added (Figs. S5(a) and (b)). We then applied negative selection to sort the variants with lower fluorescence intensity when cerulenin was absent (Figs. S5(c) and (d)). The purpose of this step was to remove the escape variants that are no longer regulated by FapR. Finally, we successfully obtained a series of malonyl-CoA-responsive genetic circuits with different dynamic ranges, among which P43FD180 achieved the highest dynamic range of 6.6-fold (Fig. 4(a)). In addition, we noted that variants with an increased dynamic range have more symmetrical palindromic structures at their FapR binding sites (Fig. S5(e)). This may be due to the fact that palindromic structures enhance the affinity between the transcription factor and the binding site [27].

The response threshold determines the application range of the genetic circuit. Here, we used two strategies to adjust the response threshold in our circuit: ① changing the expression level of FapR; and ② constructing FapR mutants. First, we used the xylose inducible promoter P_{xylA} to adjust the expression level of FapR and tested its influence on the activities of the promoters P_{fabI} and P43FD180. We found that the activities of the promoters P_{fabI} and P43FD180 were still inhibited by FapR when xylose was absent (Fig. 4(b); Fig. S7 in Appendix A), indicating that the xylose-inducible promoter P_{xylA} has leaky expression [28]. In addition, the activities of the promoters P_{fabI} and P43FD180 gradually decreased with the increase in the amount of xylose, which showed that increasing the expression of FapR reduced the leaky expression of the genetic circuit. Meanwhile, as the concentration of xylose increased, the activation effect of cerulenin gradually decreased. This finding indicates that, as the expression level of FapR increased, a higher content of malonyl-CoA was required to neutralize the inhibitory effect of the overexpressed FapR. These results demonstrate that increasing the expression of FapR increased the response threshold of the genetic circuit.

We subsequently constructed a FapR mutant library using epPCR. Next, the variants were sorted by flow cytometry, and the cells were divided into four types according to their fluorescence intensities when cerulenin was present (Fig. S8(a) in Appendix A). Then, the variants were re-screened, and it was found that

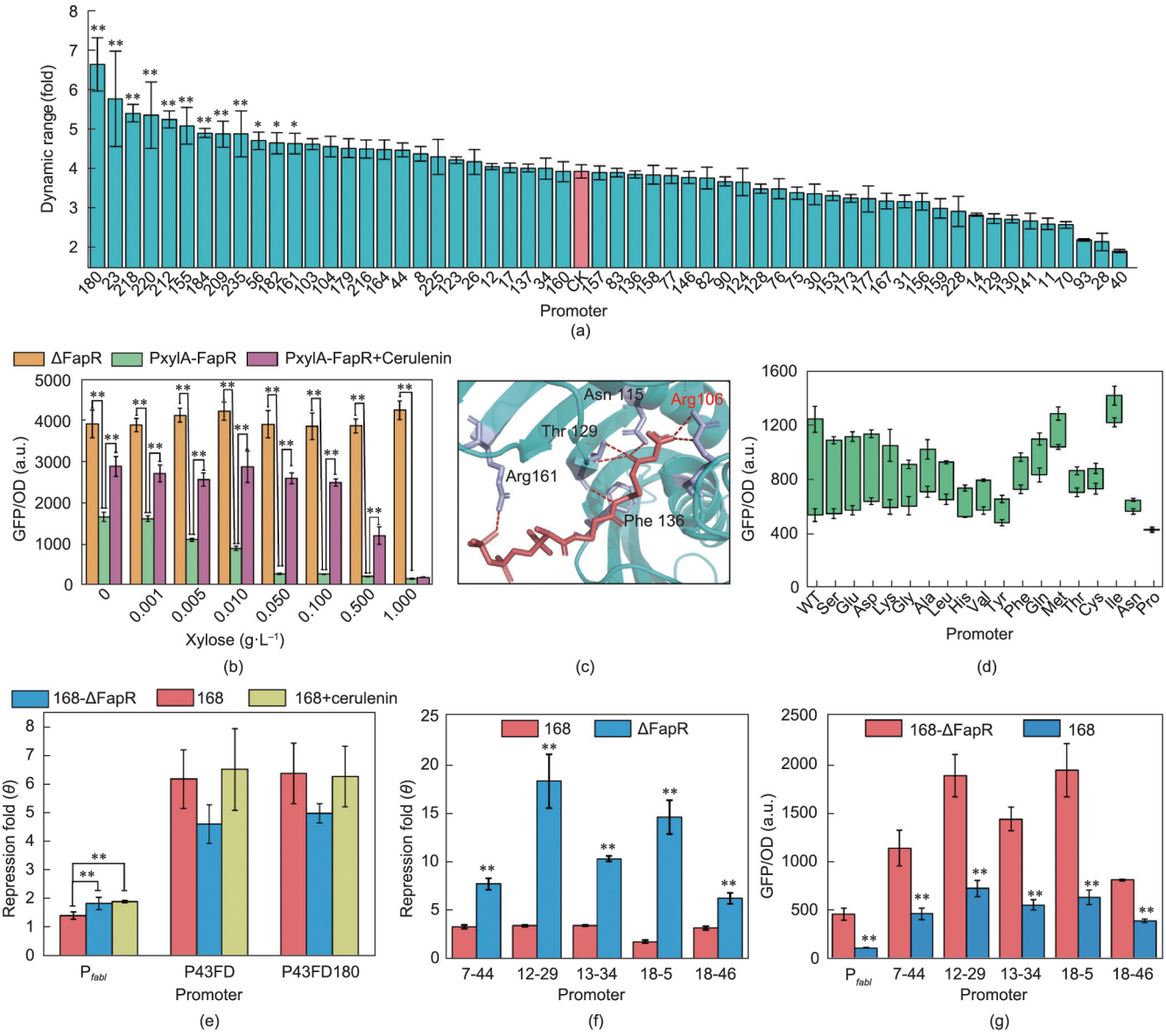

Fig. 4. Construction of bifunctional malonyl-CoA-responsive genetic circuits. (a) Dynamic range of promoter P43FD mutants, which contain different FapR boxes (CK and P43FD). (b) When adding different concentrations of xylose, the strength of the promoter P43FD180 in the different strains, respectively. ΔFapR: FapR was deleted in strain 168-ΔFapR; PxylA-FapR: FapR expression was xylose-inducible in strain 168-ΔFapR; PxylA-FapR+cerulenin: 10 μg·mL^{-1} cerulenin was added into the culture). (c) Stereo view of the FapR–malonyl-CoA complex showing the main hydrogen-bonding interaction between FapR and malonyl-CoA. The amino acids Arg106, Asn115, Thr129, Phe136, and Arg161 of FapR are involved in the interaction between FapR and malonyl-CoA. (d) Relative fluorescence intensities of P43FD180 in strains with different FapR variants (Arg106). The top and bottom of the column represent the activity of the promoter P43FD180 when 10 μg·mL^{-1} cerulenin was or was not added. WT: wild-type FapR. (e) The repression fold of the promoters P_{fabI}, P43FD, and P43FD180 as antisense promoters in strain (168) or without (168-ΔFapR) FapR, respectively. 168+cerulenin: 10 μg·mL^{-1} cerulenin was added into the culture of strain 168. (f) Repression fold of the antisense promoter FabIG variants in the strain with (168) or without (ΔFapR) FapR, respectively. (g) Strength of the FabIG variants in the strain with (168) or without (168-ΔFapR) FapR. Data displayed as mean ± s.d. (n = 3). The statistical analysis is based on Student's t-test. All data were the average of three independent experiments with standard deviations. * and ** indicate $p < 0.05$ and $p < 0.01$, respectively.

the variants with higher fluorescence intensity could no longer inhibit gene expression when cerulenin was absent. This result indicates that they had lost their regulatory function. Furthermore, the sequencing results of these variants showed that the Thr23 or Gln36 of their DNA binding domain was mutated (Fig. S8(b)), suggesting that Thr23 and Gln36 are key residues that affect the DNA binding ability of FapR. In addition, we successfully screened a variant (Arg106-Tyr) whose relative fluorescence intensity was significantly lower than that of the original strain in the presence of cerulenin. This finding demonstrated that its response threshold has been improved. Interestingly, it has been previously reported that Arg106 is one of the key residues for the binding of FapR to malonyl-CoA (Fig. 4(c)) [29]. Therefore, we decided to perform saturation mutagenesis on Arg106. The results showed that the mutation at Arg106 reduced the change in the fluorescence intensity of the genetic circuit when cerulenin was absent or present, indicating that Arg106 affects the response threshold of FapR (Fig. 4(d)).

3.4. Design and building of antisense malonyl-CoA-responsive circuits

The above constructed genetic circuits were all malonyl-CoA-activated genetic circuits. In order to expand the dynamic control capabilities, it is necessary to construct a bifunctional genetic circuit that can activate and inhibit gene expression simultaneously. So far, the ability of FapR to activate native promoter activity in *B. subtilis* has not been described; however, FapR can activate the

synthetic promoter P_{GAP} in *E. coli* [30]. Unfortunately, P_{GAP} cannot be activated by FapR in *B. subtilis* (Fig. S9 in Appendix A). Antisense transcription is a simple and universal regulatory tool, which can be used as a "NOT" gate to achieve signal conversion [25]. Therefore, we used antisense transcription to convert the malonyl-CoA-activated genetic circuit into a malonyl-CoA inhibitory genetic circuit. The malonyl-CoA-activated promoters P_{fabI}, P43FD, and P43F180 were reversed and inserted into the 3′ end of *egfp*. However, it was only when P_{fabI} was used as an antisense promoter that the inhibitory effect of antisense transcription was attenuated by FapR (Fig. 4(e)). In addition, the inhibitory effect of P_{fabI} was enhanced when cerulenin was present. However, the dynamic range of the genetic circuit P_{fabI} is only 1.3-fold. In order to improve the dynamic range of the genetic circuit, we carried out two strategies: ① The FapR binding site of P43FD180 was substituted by that of P_{fabI}, thereby generating the hybrid promoter P43FD180G; and ② the core region of the promoter P_{fabI} was substituted by the core region of the strong promoter P*grac100* to enhance the strength of P_{fabI}, creating the hybrid promoter FabIG. The results showed that, while P43FD180G cannot generate a malonyl-CoA inhibitory genetic circuit, the dynamic range of FabIG was increased by 3.0-fold (Fig. S10(a) in Appendix A).

However, when FabIG was used as an antisense promoter, it still inhibited *egfp* expression in the presence of FapR. This may be due to leaky expression of the FabIG. Recent studies have shown that, even if the antisense promoter is not active, the transcription factor binding site of the antisense promoter inhibits the expression of the forward promoter [31]. This is because the transcription factor binds to the binding site and acts as a repressor to inhibit the extension of the RNA polymerase (RNAPs) in the forward promoter. In order to verify whether the leakage inhibition effect of the genetic circuit is caused by this reason, we removed the promoter regions of the antisense promoters P43FD180, P43FD, and P_{fabI} and only retained the FapR binding site, thereby generating the promoters P43FD180Q, P43FDQ, and FaBIQ. The results showed that P43FD180Q, P43FDQ, and FabIQ inhibited the expression of *egfp* in the presence and absence of the transcription factor FapR, and the inhibitory effects were similar (Fig. S10(b)). This result indicates that the binding of FapR to the binding site does not inhibit the transcription of the forward promoter. The inhibitory effect of P43FD180Q, P43FDQ, and FabIQ on *egfp* expression could be due to the palindrome structure of the FapR binding site (Fig. S10(c)). The palindromic structure of the 3' untranslated region could affect the expression level of gene [32]. In summary, the leaky inhibition effect of the genetic circuit was a combination of the leakage expression of the antisense promoter and the palindrome structure of the FapR binding site.

Subsequently, to further improve the dynamic range of the genetic circuit, we mutated the surrounding sequence of the –35 region of FabIG to construct a promoter library. Five variants—that is, 7-44, 12-29, 13-34, 18-5, and 18-46 with dynamic ranges of 2.3-, 5.4-, 3.0-, 8.2-, and 1.9-fold, respectively—were successfully obtained (Fig. 4(f); Fig. S11 in Appendix A). Among them, the dynamic ranges of 12-29 and 18-5 were higher than that of FabIG. Finally, we tested the expression characteristics of the promoters 7-44, 12-29, 13-34, 18-5, and 18-46 (Fig. 4(g)). The result showed that their activity in strain 168-ΔFapR were higher than those of P_{fabI}, which indicates that increasing the activity of antisense promoters is an effective strategy for optimizing the dynamic range of genetic circuits.

3.5. Construction and optimization of an AND gate circuit in response to pyruvate and malonyl-CoA

PdhR is a pyruvate-responsive transcription factor in *E. coli*, and its regulatory mechanism is similar to that of FapR [33]. In order to construct a two-input AND gate responsive to pyruvate and malonyl-CoA, we inserted FapR Box180 into the downstream of the –10 region of the pyruvate-responsive promoters yteJU and yteJM, which were constructed based on PdhR in our previous study [25]. In this way, the hybrid promoters AyteJU-P43FD180 and AyteJM-P43FD180 were obtained. It is only when malonyl-CoA and pyruvate are present simultaneously that the inhibitory effects of the FapR and PdhR are released, and then the promoter will start transcription (Fig. 5(a)). Next, we detected the relative fluorescence intensities of the promoters in four strains with different genotypes, including *B. subtilis* 168 (+*fapR*, −*pdhR*), 168-ΔFapR (−*fapR*, −*pdhR*), PR (+*fapR*, +*pdhR*), and PR-ΔFapR (−*fapR*, +*pdhR*). The results showed that the activities of AyteJU-P43FD180 and AyteJM-P43FD180 in strains *B. subtilis* 168 (+*fapR*, −*pdhR*) and PR-ΔFapR (−*fapR*, +*pdhR*) were significantly lower than those in 168-ΔFapR (−*fapR*, −*pdhR*). In addition, their activities in strain PR (+*fapR*, +*pdhR*) were the lowest (Fig. S12). These finding demonstrate that both FapR and PdhR maintain their inhibitory function and, when both are present, they have a synergistic effect and reduce the leakiness of the promoters [34]. The dynamic ranges of AyteJU-P43FD180 and AyteJM-P43FD180 were 3.0- and 12.9-fold, respectively. In addition, we found that the simultaneous addition of pyruvate and cerulenin (which promotes the accumulation of malonyl-CoA) significantly restored the activities of AyteJU-P43FD180 and AyteJM-P43FD180 in the strain PR (+*fapR*, +*pdhR*) (Fig. S12). However, adding only pyruvate or cerulenin also slightly activated the promoter activity in PR. These results indicate that we successfully constructed two-input AND gates that can respond to pyruvate and malonyl-CoA. However, a certain level of leaky expression was observed when only one inducer was added.

In order to improve the dynamic range and reduce the leaky expression of the AND gates, the core region of AyteJU-P43FD180 and AyteJM-P43FD180 was replaced by the core region of the strong promoter P*grac100* to construct AyteJUG-P43FD180 and AyteJMG-P43FD180, respectively. Their dynamic ranges reached 9.8- and 8.7-fold, respectively, and the leakiness was reduced (Fig. S13 in Appendix A). In addition, the logic behaviors of AyteJUG-P43FD180 and AyteJMG-P43FD180 were more similar to an AND gate (a = 0, l = 1) than those of AyteJU-P43FD180 and AyteJM-P43FD180, due to their reduced leakiness (Fig. 5(b)). However, even when both pyruvate and cerulenin were present, the activities of AyteJUG-P43FD180 and AyteJMG-P43FD180 in PR (+*fapR*, +*pdhR*) were not fully activated (Fig. 5(c); Fig. S14). This result indicates that the inhibitory effects of PdhR and FapR were not completely released. According to the results shown in Fig. S13, the activities of AyteJUG-P43FD180 and AyteJMG-P43FD180 in *B. subtilis* 168 (+*fapR*, −*pdhR*) were completely induced by cerulenin, whereas their activities in PR-ΔFapR (−*fapR*, +*pdhR*) were not fully induced by pyruvate. These results indicate that the issue preventing the full induction of the AND gate was related to the performance of the transcription factor PdhR.

In order to address this issue, we first adjusted the expression level of PdhR by altering its promoter. A total of four promoters with different strengths were selected to express PdhR: namely, P43, P_{gsiB}, P_{veg}, and P43D1. Among them, P43, P_{gsiB}, and P_{veg} are constitutive promoters, and P43D1 is a pyruvate-activated promoter [25]. The results showed that, compared with P_{gsiB} and P_{veg}, P43 and P43D1 reduced the leaky expression of the AND gate (Fig. S15 in Appendix A). Subsequently, a flow cytometer was used to analyze the fluorescence intensity distribution of the genetic circuit. The results showed that AND gate was more homogeneous when P43D1 was used to express PdhR (Fig. 5(d)). This finding indicates that the use of self-inducible promoters to express PdhR reduces the expression noise of the genetic circuit, which is consistent with previous results [35]. In nature, the expression of most

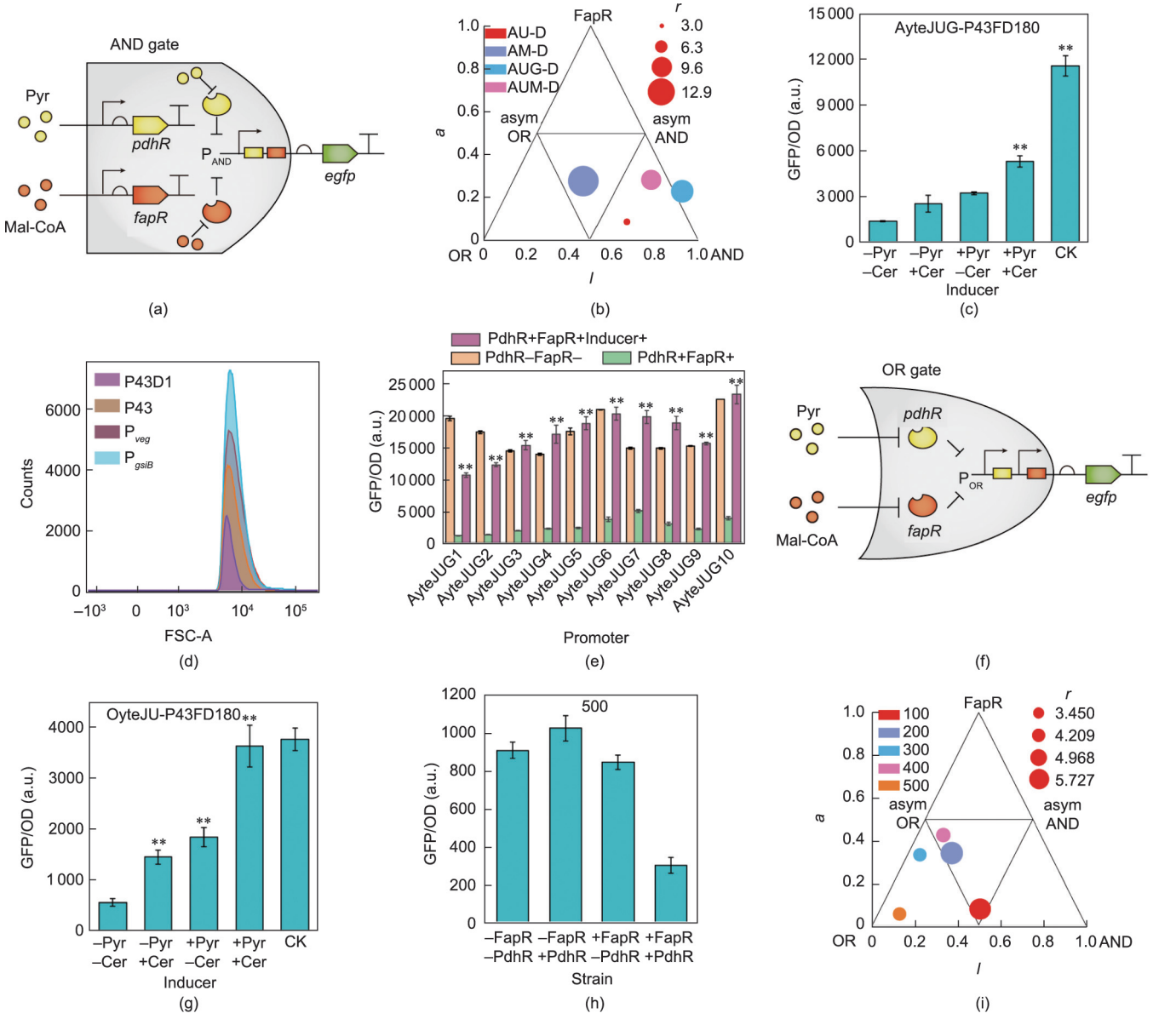

Fig. 5. Construction and optimization of the two-input AND or OR gate circuit in response to pyruvate and malonyl-CoA. (a) Schematic diagram the construction of a two-input AND gate circuit in response to pyruvate and malonyl-CoA. Yellow box: PdhR binding site; orange box: FapR binding site; Mal-CoA: malonyl-CoA. (b) Modeling results of the AND gate. The triangle plot shows three metrics of gate behavior: *r*: dynamic range; *a*: the asymmetry of the gate with respect to its two inducers; and *l*: the logical behavior of the promoter (pure AND gate ($a = 0, l = 1$); pure OR gate ($a = 0, l = 0$); pure FapR gate ($a = 1, l = 0.5$, indicates gate is only regulated by FapR); greater *a* values mean that the gate is only regulated by one of the two transcription factors). AU-D: AyteJU-FapR180D; AM-D: AyteJM-FapR180D; AUG-D: AyteJUG-FapR180D; AMG-D: AyteJMG-FapR180D. (c) Activity of AyteJUG-P43FD180 under different inducers in strain 168-PR. CK: the activity of AyteJU-P43FD180 in strain 168-ΔFapR; Pyr: 10 g·L^{-1} pyruvate; Cer: 10 μg·mL^{-1} cerulenin. (d) Effect of different promoters expressing PdhR on the fluorescence intensity distribution of strains containing AyteJU-P43FD180. (e) Dynamic range of two-input AND gate with different distances between the "–35" region and PdhR binding site. (f) Schematic diagram of the construction of a two-input OR gate circuit in response to pyruvate and malonyl-CoA. (g) Activity of OyteJU-P43FD180 under different inducers in the strain 168-PR. CK: the activity of OyteJU-P43FD180 in strain 168-ΔFapR. (h) Activity of the OR gate (OyteJU500-P43FD180) in different strains500: OyteJU500-P43FD180 when the distance between tandem promoters reached 500 bp. (i) Modeling results of the OR gate. Data displayed as mean ± s.d. ($n = 3$). The statistical analysis is based on Student's *t*-test. All data were the average of three independent experiments with standard deviations. ** indicates $p < 0.01$.

transcription factors is also self-regulated, such as GlnR and GltR [36,37], which suggests that this type of regulation may be beneficial to maintaining the stability of the entire cell regulatory network. Finally, we adjusted the distance between the PdhR binding site and the –35 region in AyteJU-P43FD180 and AyteJUG-P43FD180. The results showed that AyteJU9-P43FD180 and AyteJUG2-P43FD180 have the highest dynamic ranges of 9.1- and 17.3-fold, respectively. In addition, almost all circuits were completely activated by pyruvate and cerulenin (Fig. 5(e); Figs. S16 and S17 in Appendix A).

3.6. Construction and optimization of an OR gate circuit in response to pyruvate and malonyl-CoA

In order to construct a two-input OR gate responsive to pyruvate and malonyl-CoA, we inserted the pyruvate-activated promoter yteJU into the downstream or upstream part of the malonyl-CoA-activated promoter P43FD180, thereby generating the tandem promoters OP43FD180-yteJU and OyteJU-P43FD180. We expected that, when one of the promoters is activated by the inducer, the expression of downstream genes can be initiated

(Fig. 5(f)). The results showed that the relative fluorescence intensities of OP43FD180-yteJU and OyteJU-P43FD180 in strain PR (+*fapR*, +*pdhR*) were significantly lower than those in 168-ΔFapR (−*fapR*, −*pdhR*), *B. subtilis* 168 (+*fapR*, −*pdhR*), and PR-ΔFapR (−*fapR*, +*pdhR*) when the inducer was absent (Fig. S18 in Appendix A). This finding indicates that it is only when both transcription factors were present that the activity of the promoter was inhibited. In addition, we found that the relative fluorescence intensities of OP43FD180-yteJU and OyteJU-P43FD180 in *B. subtilis* 168 (+*fapR*, −*pdhR*) and PR-ΔFapR (−*fapR*, +*pdhR*) were significantly lower than in 168-ΔFapR (−*fapR*, −*pdhR*). Moreover, when one of the inducers (pyruvate or cerulenin) was present, the relative fluorescence intensities of OP43FD180-yteJU and OyteJU-P43FD180 in strain PR (+*fapR*, +*pdhR*) significantly increased, although they were still lower than when both inducers are present (Fig. 5(g); Fig. S19 in Appendix A). These results demonstrate that we have successfully constructed two-input OR gates that can respond to pyruvate and malonyl-CoA. However, the activity of the OR gate when one inducer was present was lower than that when two inducers were present, which may be due to the fact that the two promoters in tandem can synergistically enhance the transcription of downstream genes [38].

In order to reduce the synergistic effect of tandem promoters, we changed the distance between the two promoters. By inserting different lengths of *yeeZ* gene fragments between the promoters yteJU and P43FD180, the OR gate circuits OyteJU100-P43FD180, OyteJU200-P43FD180, OyteJU300-P43FD180, OyteJU400-P43FD180, and OyteJU500-P43FD180 were constructed. The results showed that the activity of the tandem promoter gradually decreased with the increase in the distance between the two promoters (Fig. 5(h); Fig. S20 in Appendix A). In addition, according to the modeling results, better OR behaviors were obtained when the distance between two promoters increased (Fig. 5(i); Fig. S21 in Appendix A). The dynamic range of the OR gate was increased by 5.6-fold (OyteJU200-P43FD180).

3.7. Remodeling IPP metabolism using the TIMO genetic circuits

We next used these genetic circuits to build a cascade regulatory system for dynamically remodeling the IPP metabolism in the strain BS17-MVA (Fig. 2(f); Fig. S22 in Appendix A). We divided the metabolic network into three modules: namely, the central metabolism module, IPP supply module (MVA+MEP pathway), and terpenoids synthesis module. First, in the central metabolism module, two pyruvate-activated promoters (D11, D6) with different dynamic ranges were used to dynamically enhance the expression of pyruvate dehydrogenase PdhA, while two malonyl-CoA-inhibited promoters (FabIG18-5 and FabIG12-29) with different dynamic ranges were used to dynamically inhibit the expression of AccA and citrate synthase CitZ. Then, for the IPP supply module, three pyruvate-malonyl-CoA 2-input AND gates (AyteJM-P43FD180, AyteJU9-P43FD180, and AyteJUG2-P43FD180) or OR gates (OyteJU-P43FD180, OyteJU300-P43FD180, and OyteJU500-P43FD180) with different dynamic ranges were used to dynamically enhance the expression of the 1-deoxy-D-xylulose-5-phosphate synthase Dxs and acetoacetyl-CoA thiolase MvaE. As the result, the titer of MK-7 in strain BS17-P13 (203.7 mg·L^{-1}) was increased by 135.8% compared with that of strain BS17-MVA (Fig. 6(a)). In addition, in the strain BS17-P13, the AND gate (AyteJUG2-P43FD180) was used to control the expression of the enzymes Dxs and MvaE. As shown in Fig. S23 in Appendix A, the glucose consumption rates of strains P12, P17, and P18 were significantly lower than those of the other strains. Furthermore, the MK-7 titer of strain P12 was significantly lower than that of P11 and P13 (the parallel strains regulated by AND gates of different strengths). The MK-7 titer of strains P17 and P18 was significantly lower than that of P19 (the parallel strain regulated by AND gates of different strengths). These results indicated that the strains P12, P17, and P18 could not effectively convert glucose into MK-7, so their glucose consumption was lower. In addition, we found that the lower MK-7 titer of strains P10 and P12 may be due to their lower intracellular concentration of acetyl-CoA, MVA, MEP, and IPP; their high pyruvate:acetyl-CoA ratio; and their imbalance of central metabolic fluxes (Fig. S24 in Appendix A). This phenomenon demonstrated that the simultaneous control of the metabolic fluxes of the MEP and MVA modules promotes the synthesis of terpenoids. As the control, if PdhR and FapR were not present in the strain expressing the genetic circuit, the highest titer of MK-7 (strain BS17-F5) relative to strain BS17-MVA was only increased by 30% (112.4 mg·L^{-1}).

To further increase MK-7 production, the AND gate (AyteJUG2-P43FD180) was introduced into the strain BS17-P13 to dynamically activate the expression of heptamyl diphosphate synthase (HepTS) in the MK-7 biosynthesis pathway, generating the strain BS17-P20, which produced up to 467.2 mg·L^{-1} MK-7 in the shake flask. In addition, we found that the intracellular levels of MVA (78.18 nmol·g^{-1} DCW), MEP (161.58 nmol·g^{-1} DCW), and IPP (1.50 nmol·g^{-1} DCW) in strain BS17-P20 increased by 28.6-, 15.3-, and 4-fold at 48 h, respectively, compared with those of BS17-MVA (Fig. 6(b); Fig. S25 in Appendix A). Meanwhile, the intracellular levels of acetyl-CoA (364.60 nmol·g^{-1} DCW) and pyruvate (1213.20 nmol·g^{-1} DCW) in strain BS17-P20 decreased by 25.0% and 32.0% compared with those in BS17-MVA, respectively (Fig. 6(c); Fig. S26 in Appendix A). Furthermore, the intracellular content ratio between MEP and MVA in strain BS17-P20 (3.3:1) decreased compared with that in BS17-MVA (6.3:1). These results demonstrate that the constructed cascade regulatory framework remodeled the IPP metabolism, thereby promoting the overproduction of MK-7. In addition, we found that the increase in MK-7 production was not positively related to the promoter strength that controls the MVA and the MEP expression, since some of the promoters used were weaker than the original one. This finding further suggests that the increase in IPP content is caused by the cooperative regulation of the circuit. The IPP content in strain BS17-P20 (368.8 pg·mg^{-1}) was higher than that in many plants, including the model plants *Arabidopsis thaliana* (1.1 pg·mg^{-1}), *Nicotiana attenuate* (32.2 pg·mg^{-1}), and *Picea abies* (303.7 pg·mg^{-1}) [39].

Subsequently, we constructed a *de novo* synthetic pathway for the production of the terpenoid β-carotene in BS17-MVA and BS17-P13 to further validate the function of the TIMO genetic circuits-assisted IPP metabolism remodeling framework (Fig. 6(d)). The enzymes geranylgeranyl diphosphate synthase (CrtE), phytoene synthase (CrtB), phytoene desaturase (CrtI), and lycopene β-cyclase (CrtY) from *E. herbicola* Eho10 were expressed in the low copy number plasmid pHT01 and transformed into the strains BS17-MVA and BS17-P13, yielding the strains MVA-Beta and P13-Beta, respectively (Fig. 6(d)). The titer of β-carotene in strain P13-Beta (0.53 mg·L^{-1}) was 1.9 times that in strain MVA-Beta (0.28 mg·L^{-1}). The titer of intermediate lycopene in strain P13-Beta (4.10 mg·L^{-1}) was ten times that in strain MVA-Beta (0.41 mg·L^{-1}) (Fig. 6(d); Fig. S27 in Appendix A). These results demonstrate that the cascade regulatory system constructed here can also enhance the production of other terpenoids.

It is known that the robustness of genetic circuits may be poor in large-scale fermentation. For example, the introduction of a quorum-sensing molecular switch into the strain BS17 increased the titer of MK-7 to 360 mg·L^{-1} in a shake flask, but dropped it to 200 mg·L^{-1} in a bioreactor [17]. Finally, in order to test the stability of the TIMO genetic circuits-assisted IPP metabolism remodeling framework in large-scale fermentation, the strain BS17-P20 was further used for the production of MK-7 in a 50-L bioreactor.

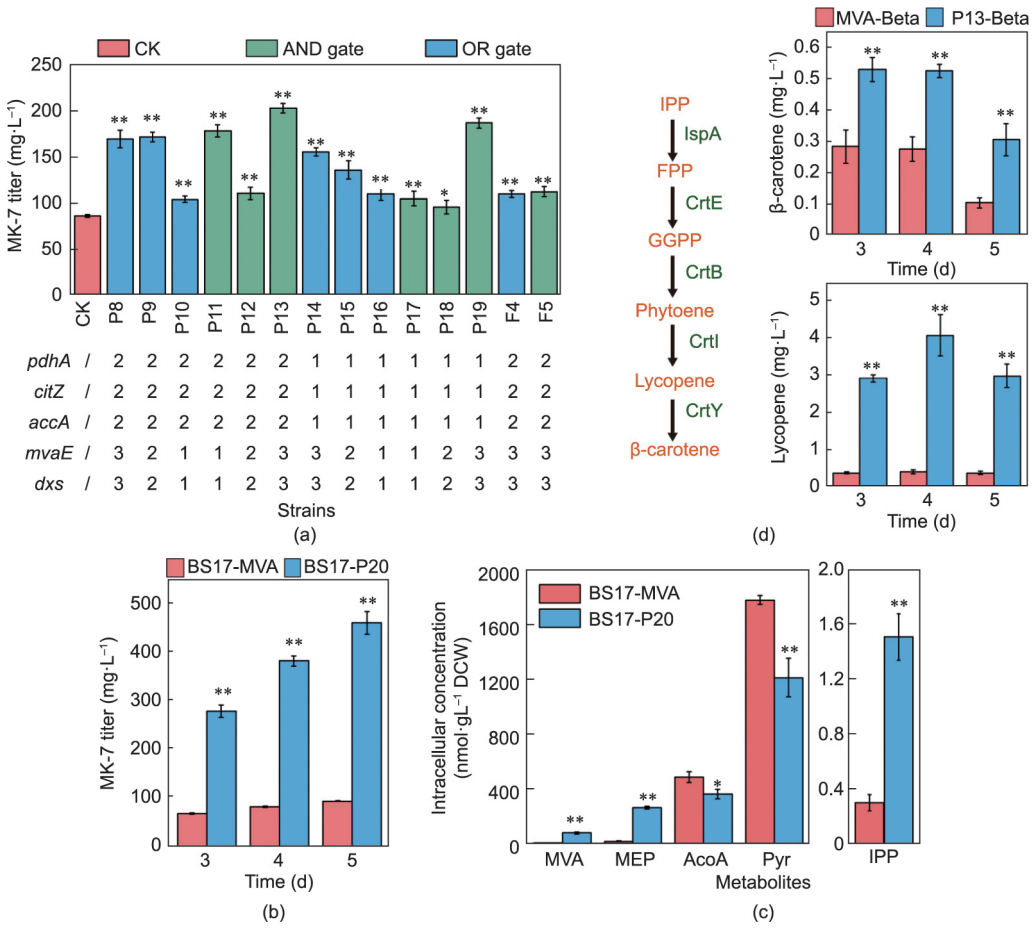

Fig. 6. Dynamic control of MK-7 synthesis. (a) Effects of dynamically regulating the central metabolism module and IPP supply module/MK-7 synthesis module on the titer of MK-7. CK: strain BS17-MVA; P8-P19: dynamically regulated strains; F4-F5: statically regulated strains. 1, 2, 3 indicates that the intensity of the regulation is stepwise enhanced; *pdhA*: pyruvate-activated promoters D6 (1) and D11 (2); *accA* and *citZ*: malonyl-CoA-inhibited promoters FabIG18-5 (1) and FabIG12-29 (2); *mvaE* and *dxs*: pyruvate-malonyl-CoA 2-input AND gates AyteJM-P43FD180 (1), AyteJU9-P43FD180 (2), AyteJUG2-P43FD180 (3) or OR gates OyteJU500-P43FD180 (1), OyteJU300-P43FD180 (2) and OyteJU-P43FD180 (3). (b) MK-7 titer of the strains BS17-MVA and BS17-P20 at different fermentation times. (c) Intracellular content of MEP, MVA, and acetyl-CoA, pyruvate, and IPP in the strains BS17-MVA and BS17-P20 at 48 h. Pyr: pyruvate; Aco: acetyl-CoA. (d) Construction of the β-carotene biosynthesis pathway in the strains BS17-MVA and BS17-P13. Titer of β-carotene and lycopene in the strains MVA-Beta and P13-Beta at different fermentation times. CrtE: geranylgeranyl diphosphate synthase; CrtB: phytoene synthase; CrtI: phytoene desaturase; CrtY: lycopene β-cyclase; FPP: farnesyl diphosphate; GGPP: geranylgeranyl diphosphate; Data displayed as mean ± s.d. (n = 3). The statistical analysis is based on Student's t-test. All data were the average of three independent experiments with standard deviations. * and ** indicate $p < 0.05$ and $p < 0.01$, respectively.

The concentration of glucose in the bioreactor was maintained at 20–30 g·L^{-1}, and the maximum OD_{600} of the strain reached 83.6 at 56 h. After 132 hours of fermentation, the titer of MK-7 reached 1549.6 mg·L^{-1}, which is the highest production of MK-7 reported to date (Fig. S28 in Appendix A).

4. Conclusions

Overall, we successfully remodeled and synergistically regulated the IPP metabolism by using TIMO genetic circuits-assisted cascade regulatory systems that respond to pyruvate and malonyl-CoA in *B. subtilis*. We also demonstrated the universality and robustness of the framework. This regulatory system provides an alternative strategy for remodeling the IPP metabolism in other chassis cells. In addition, this study demonstrates the potential of using multi-signal, coordinated, and cascaded dynamic regulation strategies to rationally and globally fine-tune complex metabolic pathways, which may be useful for the production of other chemicals.

Acknowledgments

This work was financially supported by the National Natural Science Foundation of China (32070085, 32200050, 31871784, and 32021005), the Natural Science Foundation of Jiangsu Province (BK20221079), National Postdoctoral Program for Innovative Talents (BX20220136), the Jiangsu Funding Program for Excellent Postdoctoral Talent (2022ZB498), the Fundamental Research Funds for the Central Universities (JUSRP52019A, JUSRP121010 and JUSRP221013), National Key Research and Development Program of China (2020YFA0908300), and Postgraduate Research & Practice Innovation Program of Jiangsu Provence (KYCX18_1797).

Compliance with ethics guidelines

Xianhao Xu, Xueqin Lv, Shixiu Cui, Yanfeng Liu, Hongzhi Xia, Jianghua Li, Guocheng Du, Zhaofeng Li, Rodrigo Ledesma-Amaro, Jian Chen, and Long Liu declare that they have no conflict of interest or financial conflicts to disclose.

Appendix A. Supplementary data

Supplementary data to this article can be found online at https://doi.org/10.1016/j.eng.2023.03.019.

References

[1] Li M, Hou F, Wu T, Jiang X, Li F, Liu H, et al. Recent advances of metabolic engineering strategies in natural isoprenoid production using cell factories. Nat Prod Rep 2020;37(1):80–99.
[2] Denby CM, Li RA, Vu VT, Costello Z, Lin W, Chan LJG, et al. Industrial brewing yeast engineered for the production of primary flavor determinants in hopped beer. Nat Commun 2018;9:965.
[3] Daletos G, Katsimpouras C, Stephanopoulos G. Novel strategies and platforms for industrial isoprenoid engineering. Trends Biotechnol 2020;38(7):811–22.
[4] Paddon CJ, Keasling JD. Semi-synthetic artemisinin: a model for the use of synthetic biology in pharmaceutical development. Nat Rev Microbiol 2014;12(5):355–67.
[5] Chen Y, Daviet L, Schalk M, Siewers V, Nielsen J. Establishing a platform cell factory through engineering of yeast acetyl-CoA metabolism. Metab Eng 2013;15:48–54.
[6] Wang C, Zada B, Wei G, Kim SW. Metabolic engineering and synthetic biology approaches driving isoprenoid production in *Escherichia coli*. Bioresour Technol 2017;241:430–8.
[7] Xie W, Lv X, Ye L, Zhou P, Yu H. Construction of lycopene-overproducing *Saccharomyces cerevisiae* by combining directed evolution and metabolic engineering. Metab Eng 2015;30:69–78.
[8] Ajikumar PK, Xiao WH, Tyo KE, Wang Y, Simeon F, Leonard E, et al. Isoprenoid pathway optimization for Taxol precursor overproduction in *Escherichia coli*. Science 2010;330(6000):70–4.
[9] Lv X, Xie W, Lu W, Guo F, Gu J, Yu H, et al. Enhanced isoprene biosynthesis in *Saccharomyces cerevisiae* by engineering of the native acetyl-CoA and mevalonic acid pathways with a push–pull–restrain strategy. J Biotechnol 2014;186:128–36.
[10] Yang C, Gao X, Jiang Y, Sun B, Gao F, Yang S. Synergy between methylerythritol phosphate pathway and mevalonate pathway for isoprene production in *Escherichia coli*. Metab Eng 2016;37:79–91.
[11] Wang X, Han J, Zhang X, Ma Y, Lin Y, Wang H, et al. Reversible thermal regulation for bifunctional dynamic control of gene expression in *Escherichia coli*. Nat Commun 2021;12:1411.
[12] Hossain GS, Saini M, Miyake R, Ling H, Chang MW. Genetic biosensor design for natural product biosynthesis in microorganisms. Trends Biotechnol 2020;38(7):797–810.
[13] Jones TS, Oliveira SMD, Myers CJ, Voigt CA, Densmore D. Genetic circuit design automation with Cello 2.0. Nat Protoc 2022;17(4):1097–113.
[14] Chou HH, Keasling JD. Programming adaptive control to evolve increased metabolite production. Nat Commun 2013;4:2595.
[15] Zhou S, Yuan S, Nair PH, Alper HS, Deng Y, Zhou J. Development of a growth coupled and multi-layered dynamic regulation network balancing malonyl-CoA node to enhance (2S)-naringenin biosynthesis in *Escherichia coli*. Metab Eng 2021;67:41–52.
[16] Scheiber D, Veulemans V, Horn P, Chatrou ML, Potthoff SA, Kelm M, et al. High-dose menaquinone-7 supplementation reduces cardiovascular calcification in a murine model of extraosseous calcification. Nutrients 2015;7(8):6991–7011.
[17] Cui S, Lv X, Wu Y, Li J, Du G, Ledesma-Amaro R, et al. Engineering a bifunctional phr60-rap60-spo0A quorum-sensing molecular switch for dynamic fine-tuning of menaquinone-7 synthesis in *Bacillus subtilis*. ACS Synth Biol 2019;8(8):1826–37.
[18] Zhang X, Cui Z, Hong Q, Li S. High-level expression and secretion of methyl parathion hydrolase in *Bacillus subtilis* WB800. Appl Environ Microbiol 2005;71(7):4101–3.
[19] Cox RS, Surette MG, Elowitz MB. Programming gene expression with combinatorial promoters. Mol Syst Biol 2007;3:145.
[20] Onorato JM, Chen L, Shipkova P, Ma Z, Azzara AV, Devenny JJ, et al. Liquid–liquid extraction coupled with LC/MS/MS for monitoring of malonyl-CoA in rat brain tissue. Anal Bioanal Chem 2010;397(7):3137–42.
[21] Kindt E, Szekely-Klepser G, Fountain ST. The validation of a simple LC/MS/MS method for determining the level of mevalonic acid in human plasma. Biomed Chromatogr 2011;25(3):323–9.
[22] Buescher JM, Moco S, Sauer U, Zamboni N. Ultrahigh performance liquid chromatography-tandem mass spectrometry method for fast and robust quantification of anionic and aromatic metabolites. Anal Chem 2010;82(11):4403–12.
[23] Gao Q, Chen H, Wang G, Yang W, Zhong X, Liu J, et al. Highly efficient production of menaquinone-7 from glucose by metabolically engineered *Escherichia coli*. ACS Synth Biol 2021;10(4):756–65.
[24] Commichau FM, Forchhammer K, Stülke J. Regulatory links between carbon and nitrogen metabolism. Curr Opin Microbiol 2006;9(2):167–72.
[25] Xu X, Li X, Liu Y, Zhu Y, Li J, Du G, et al. Pyruvate-responsive genetic circuits for dynamic control of central metabolism. Nat Chem Biol 2020;16(11):1261–8.
[26] Albanesi D, de Mendoza D, Fap R. From control of membrane lipid homeostasis to a biotechnological tool. Front Mol Biosci 2016;3:64.
[27] Li J, Dai S, Chen X, Liang X, Qu L, Jiang L, et al. Mechanism of forkhead transcription factors binding to a novel palindromic DNA site. Nucleic Acids Res 2021;49(6):3573–83.
[28] Bhavsar AP, Zhao X, Brown ED. Development and characterization of a xylose-dependent system for expression of cloned genes in *Bacillus subtilis*: conditional complementation of a teichoic acid mutant. Appl Environ Microbiol 2001;67(1):403–10.
[29] Schujman GE, Guerin M, Buschiazzo A, Schaeffer F, Llarrull LI, Reh G, et al. Structural basis of lipid biosynthesis regulation in Gram-positive bacteria. EMBO J 2006;25(17):4074–83.
[30] Xu P, Li L, Zhang F, Stephanopoulos G, Koffas M. Improving fatty acids production by engineering dynamic pathway regulation and metabolic control. Proc Natl Acad Sci USA 2014;111(31):11299–304.
[31] Hao N, Palmer AC, Ahlgren-Berg A, Shearwin KE, Dodd IB. The role of repressor kinetics in relief of transcriptional interference between convergent promoters. Nucleic Acids Res 2016;44(14):6625–38.
[32] Court DL, Gan J, Liang Y, Shaw G, Tropea JE, Costantino N, et al. RNase III: genetics and function; structure and mechanism. Annu Rev Genet 2013;47:405–31.
[33] Feng Y, Cronan JE. PdhR, the pyruvate dehydrogenase repressor, does not regulate lipoic acid synthesis. Res Microbiol 2014;165(6):429–38.
[34] Bordoy AE, O'Connor NJ, Chatterjee A. Construction of two-input logic gates using transcriptional interference. ACS Synth Biol 2019;8(10):2428–41.
[35] Isaacs FJ, Hasty J, Cantor CR, Collins JJ. Prediction and measurement of an autoregulatory genetic module. Proc Natl Acad Sci USA 2003;100(13):7714–9.
[36] Fisher SH, Wray LV. *Bacillus subtilis* glutamine synthetase regulates its own synthesis by acting as a chaperone to stabilize GlnR-DNA complexes. Proc Natl Acad Sci USA 2008;105(3):1014–9.
[37] Belitsky BR, Sonenshein AL. Altered transcription activation specificity of a mutant form of *Bacillus subtilis* GltR, a LysR family member. J Bacteriol 1997;179(4):1035–43.
[38] Liu Z, Zheng W, Ge C, Cui W, Zhou L, Zhou Z. High-level extracellular production of recombinant nattokinase in *Bacillus subtilis* WB800 by multiple tandem promoters. BMC Microbiol 2019;19(1):89.
[39] Krause T, Reichelt M, Gershenzon J, Schmidt A. Analysis of the isoprenoid pathway intermediates, dimethylallyl diphosphate and isopentenyl diphosphate, from crude plant extracts by liquid chromatography tandem mass spectrometry. Phytochem Anal 2020;31(6):770–7.